



Cite this: *Phys. Chem. Chem. Phys.*,  
2023, 25, 28955

# Release of molecules from nanocarriers

Vladimir P. Zhdanov<sup>ab</sup>

Release of drugs or vaccine molecules from macro-, micro-, and nano-sized carriers is usually considered to be limited by diffusion and/or carrier dissolution and/or erosion. The corresponding experimentally observed kinetics are customarily fitted by using the empirical Weibull and Korsmeyer–Peppas expressions. With decreasing size of carriers down to about 100 nm, the timescale of diffusion decreases, and accordingly the release can be kinetically limited, *i.e.*, controlled by jumps of molecules located near the carrier–solution interface. In addition, nanocarriers (*e.g.*, lipid nanoparticles) are often structurally heterogeneous so that the absorption of molecules there can be interpreted in terms of energetic heterogeneity, *i.e.*, distribution of energies corresponding to binding sites and activation barriers for release. Herein, I present a general kinetic model aimed at such situations. For illustration, the deviation of the molecule binding energy from the maximum value was considered to be about 4–8 kcal mol<sup>−1</sup>. With this physically reasonable (for non-covalent interaction) scale of energetic heterogeneity, the predicted kinetics (i) are linear in the very beginning and then, with increasing time, become logarithmic and (ii) can be nearly perfectly fitted by employing the Weibull or Korsmeyer–Peppas expressions with the exponent in the range from 0.6 to 0.75. Such values of the exponent are often obtained in experiments and customarily associated with non-Fickian diffusion. My analysis shows that the energetic heterogeneity can be operative here as well.

Received 23rd April 2023,  
Accepted 11th September 2023

DOI: 10.1039/d3cp01855e

rsc.li/pccp

## 1. Introduction

Release of molecules from macro-, micro-, and nanocarriers is a very general phenomenon occurring in various branches of natural science and playing an important role in numerous applications. One of the best practically important examples is drug release. Usually, it occurs from macroscopic pellets (reviewed in ref. 1–3). Nowadays, however, attention is shifted to the fabrication of novel drugs and antiviral vaccines based, *e.g.*, on RNA (mRNA or siRNA) delivery by nanocarriers such as 100 nm-sized lipid nanoparticles (LNPs; reviewed in ref. 4–6). In the corresponding experiments, one typically measures the release kinetics. The interpretation and/or fitting of such kinetics is customarily based on the use of the analytical expressions predicted by generic models or validated empirically (reviewed in ref. 7–9; see also below).

One of the key generic models implies that the release is limited by Fickian diffusion of molecules towards the carrier–solution interface. For spherically-shaped homogeneous carriers, the textbook solution of the corresponding diffusion equation using the eigenfunction method (*e.g.*, ref. 9 and 10) yields the following expression for the dependence of the normalized

amount of released drug or vaccine,  $M(t)/M_\infty$  ( $M_\infty$  is the value corresponding to  $t \rightarrow \infty$ ), on time,  $t$ ,

$$\varphi(t) \equiv \frac{M(t)}{M_\infty} = 1 - \sum_{m=1}^{\infty} \frac{6}{\pi^2 m^2} \exp\left(-\frac{D\pi^2 m^2 t}{R^2}\right), \quad (1)$$

where  $D$  is the drug diffusion coefficient,  $R$  is the carrier radius, and  $m$  are integers corresponding to different eigenfunctions. For the very initial phase of the release, the value of  $\varphi$  is determined by many eigenfunctions, and the model predicts

$$\varphi \simeq 6\left(\frac{Dt}{\pi R^2}\right)^{1/2}, \quad (2)$$

whereas afterwards the eigenfunction with  $m = 1$  dominates, and (1) is reduced to

$$\varphi \simeq 1 - \frac{6}{\pi^2} \exp\left(-\frac{D\pi^2 t}{R^2}\right). \quad (3)$$

A more universal empirical expression for  $\varphi$  is

$$\varphi = 1 - \exp(-Bt^\alpha), \quad (4)$$

where  $B$  and  $\alpha$  are parameters. This expression is usually attributed to Weibull<sup>11</sup> who proposed it in contexts not related to drug release. In applications, one often has  $\alpha \leq 1$ . The larger values,  $\alpha > 1$ , were sometimes reported as well (see *e.g.* ref. 12).

The most frequently applied empirical power-law expression attributed often in the area under consideration to Korsmeyer

<sup>a</sup> Section of Nano and Biophysics, Department of Physics, Chalmers University of Technology, Göteborg, Sweden. E-mail: zhdanov@chalmers.se

<sup>b</sup> Boreskov Institute of Catalysis, Russian Academy of Sciences, Novosibirsk, Russia. E-mail: zhdanov@catalysis.ru



and Peppas<sup>13</sup> is obtained by the linear expansion of (4) at  $Bt^\alpha \ll 1$ ,

$$\varphi = Bt^\alpha. \quad (5)$$

In experiments,  $\varphi$  often does not reach unity, and under such conditions the difference between eqn (4) and (5) is minor. Sometimes, however, eqn (5) is used to fit experimental data up to  $\varphi \simeq 1$ , *i.e.*, beyond the applicability of the expansion of eqn (4). From this perspective, eqn (4) and (5) can be considered to be independent and are customarily associated with different names.

Often, the drug release can be limited by carrier dissolution and/or erosion. For spherically-shaped homogeneous carriers, the simplest shrinking core model describing this case predicts (see, *e.g.*, ref. 14)

$$\varphi = 1 - (R - vt)^3/R^3, \quad (6)$$

where  $R$  is the initial carrier radius, and  $v$  is the dissolution or erosion rate.

In the literature, one can find many other models extending and/or complementing those mentioned above. In particular, diffusion-limited release was widely analyzed from various perspectives. Many treatments were aimed at the situations when the diffusion is Fickian whereas a carrier is either uniform but non-spherical<sup>15,16</sup> or spherically shaped but with a uniform core and one or a few uniform shells.<sup>17–21</sup> There are treatments<sup>22–25</sup> aimed at explaining why the experimentally obtained exponent in (5) is often not equal to that of  $\simeq 0.5$ , expected in the case of Fickian diffusion [eqn (2)]. The focus is there on the non-Fickian diffusion related to the carrier structural heterogeneity on the length scale much smaller than the carrier size, *e.g.*, due to the fractal-like carrier structure. The interplay of Fickian diffusion and carrier dissolution and/or erosion<sup>26–28</sup> and the release after rupture of carrier particles<sup>29</sup> were analyzed as well.

Regarding the comparison of theoretical and experimental release kinetics, one can note that the models usually imply that the size or initial size of carrier particles is fixed whereas in reality the kinetics are customarily measured at the ensemble level and represent convolution of the kinetics corresponding to the size distribution. From this perspective, the observed kinetics and/or obtained parameters are apparent and may be different compared to those corresponding to the fixed size. This effect may be important if the size distribution is appreciable<sup>16</sup> as happens *e.g.* in the case of LNPs.

Taken together, the analytical expressions used to interpret and/or fit the measured release kinetics are either empirical or imply diffusion limitations of cargo and/or dissolution of carrier. Physically, the diffusion limitations take place provided the release of molecules located near the carrier–solution interface is sufficiently fast compared to diffusion inside a carrier on the length scale comparable to the carrier size.

In the case of nanocarriers, the condition formulated above can be violated because the corresponding size is small (often  $\sim 100$  nm) and accordingly the diffusion timescale is short. An additional reason why this condition can fail in this limit is that the surface of nanoparticles is often well ordered and

accordingly the release of molecules located near the carrier–solution interface may be slower compared to the diffusion inside. In the case of LNPs, for example, the carrier–solution interface typically represents a well-formed lipid bilayer.<sup>30–32</sup> Under such circumstances, the diffusion limitations can be negligible at least sometimes, and the release can occur in the kinetically-limited regime. Another important factor is that biologically-relevant nanocarriers are often highly heterogeneous inside on the length scale much smaller than their size. For example, the poorly ordered internal part of LNPs (i) can be reminiscent of multilamellar vesicles with solution and RNA located between lipid leaflets<sup>30</sup> or (ii) exhibit more complex and less ordered domains of the “cubic” phase, formed by a lipid bilayer and containing water channels<sup>31</sup> or (iii) an “inverse hexagonal” phase.<sup>32</sup> The structural heterogeneity of such carriers is expected to result in the complexity of the network of local minima and transition states at the potential-energy landscape for diffusion and release of molecules transported by a carrier. The distributions of energies of these local minima and transition states can be relatively broad. In other words, such carriers are expected to exhibit appreciable energetic heterogeneity. In the available kinetic models focused on diffusion limitation (*e.g.*, ref. 22–25), as mentioned above, the structural heterogeneity is sometimes taken into account whereas the energetic heterogeneity is ignored.

Referring to nanocarriers, I present herein an alternative generic model implying kinetically limited release in the presence of appreciable energetic heterogeneity. This heterogeneity is described at the level of the already mentioned distributions of energies of local minima and transition states available at the potential energy surface (Section II). The diffusion of transported molecules inside a carrier is considered to be rapid (this condition corresponds to kinetically limited release) so that their distributions over sites is close to canonical. Despite this physical simplification, the corresponding general kinetic equations are rather cumbersome (Section II.A). In some practically important situations, they can be mathematically simplified (Section II.B) and used to illustrate the special features of the kinetics under consideration (Section III) and to discuss the relation of the results presented to what is observed in real systems (Sections IV and V).

## II. Model

### A. General equations

In the model under consideration, the local minima at the potential-energy landscape for the location of drug or vaccine molecules inside a carrier are identified with sites, and a carrier is viewed as a set of sites. Each site can be occupied by one molecule, and the corresponding energy of a molecule is designated as  $E$ . As mentioned in the introduction, carriers are assumed to be energetically heterogeneous, *i.e.*, there is distribution of  $E$  designated as  $F(E)$ . The minimal and maximal energies are identified with 0 and  $\Delta$ . With this specification,  $E$  represents the deviation of energy from the minimal value. The  $E$  distribution is



normalized as

$$\int_0^{\Delta} F(E) dE = 1. \quad (7)$$

The interaction between molecules is neglected and, as already noted in the introduction, the focus is on the kinetically-limited release when the jumps of molecules from occupied sites to adjacent vacant sites are rapid so that the distribution of molecules among sites is close to canonical. The corresponding probability that a site is occupied depends on  $E$  and is designated as  $p(E)$ . The fraction of occupied sites is expressed as

$$f = \int_0^{\Delta} p(E) F(E) dE. \quad (8)$$

For nanocarriers in solution, the canonical distribution is applicable, because the corresponding energy exchange is typically fast on the timescale of the carrier release.

In practically important cases, the number of molecules in a carrier is usually large ( $\gg 1$ ), and accordingly the canonical distribution can be replaced by the grand canonical distribution,

$$p(E) = \frac{\exp[(\mu - E)/k_B T]}{1 + \exp[(\mu - E)/k_B T]}, \quad (9)$$

where  $\mu$  is the chemical potential corresponding to a given value of  $f$ . By definition [eqn (8)],  $\mu$  and  $f$  are related in the form

$$f = \int_0^{\Delta} \frac{\exp[(\mu - E)/k_B T]}{1 + \exp[(\mu - E)/k_B T]} F(E) dE. \quad (10)$$

The total number of molecules in a carrier is given by

$$n = Nf, \quad (11)$$

where

$$N = V/v \quad (12)$$

is the total number of sites, whereas  $V$  and  $v$  are the carrier total volume and volume per site, respectively. For spherically-shaped carriers, we have

$$N = 4\pi R^3/3v, \quad (13)$$

where  $R$  is the corresponding radius.

The carrier volume per site,  $v$ , is introduced above formally via eqn (12) for  $N$ , i.e., it can be read as  $v = V/N$  and considered as the definition of  $v$ . In other words, a carrier is considered to be formed of sites, and the total volume of sites is equal to the carrier volume. The so-defined volume per site,  $v$ , is usually appreciably larger than the geometrical volume of a molecule.

The release of molecules from a carrier is considered to occur from some of the sites located near the carrier-solution interface. These sites form a subset of the whole set of sites, and the corresponding energy  $E$  of a molecule can also be in the range from 0 to  $\Delta$ . As usual in the Arrhenius framework, the release is described in terms of the transition of a molecule along the potential energy surface so that  $E$  corresponds to the local minimum. The rate constant of release depends on  $E$  and also on the energy of a molecule in the activated state or, more specifically, on the deviation of this energy from the minimal

value. Designating this deviation as  $E_*$ , the release rate constant is represented as

$$k(E, E_*) = k_0 \exp[-(E_* - E)/k_B T], \quad (14)$$

where  $k_0$  is the rate constant at  $E = E_* = 0$ . By analogy with  $E$ , the minimal and maximal values of  $E_*$  are identified with 0 and  $\Delta_*$ . Thus, each site located near the carrier-solution interface and allowing release is characterized by two parameters,  $E$  and  $E_*$ , and their distribution is designated to be  $\mathcal{F}(E, E_*)$ . By definition,  $\mathcal{F}(E, E_*) dE dE_*$  is the fraction of sites with the parameters in the ranges from  $E$  to  $E + dE$  and from  $E_*$  to  $E_* + dE_*$ , and the corresponding normalization is as follows

$$\int_0^{\Delta} \int_0^{\Delta_*} \mathcal{F}(E, E_*) dE_* dE = 1. \quad (15)$$

With this specification, the release rate is given by

$$w = \mathcal{N} \int_0^{\Delta} \int_0^{\Delta_*} k(E, E_*) p(E) \mathcal{F}(E, E_*) dE_* dE, \quad (16)$$

where  $p(E)$  is the occupation probability defined by (9), and

$$\mathcal{N} = S/s \quad (17)$$

is the number of sites allowing release ( $S$  is the interface area, and  $s$  is the area per such a site). For spherically-shaped carriers, we have

$$\mathcal{N} = 4\pi R^2/s. \quad (18)$$

By analogy with the definition of  $v$  in eqn (12) and (13),  $s$  has been introduced above formally, i.e., eqn (17) can be read as  $s = S/\mathcal{N}$  and considered as the definition of  $s$ . Regarding  $s$ , I can add that the carrier structure near the interface is typically different compared to that inside. In addition, not all the sites located at the interface are expected to allow release. For these reasons, the formally defined  $s$  can be appreciably larger than the average cross-sectional area of a site inside the carrier. With this reservation,  $s$  is expected to be much smaller than  $S$ .

The kinetic equation for release is

$$dn/dt = -w. \quad (19)$$

Substituting (11) and (16) into (19) yields

$$\frac{df}{dt} = -\chi \int_0^{\Delta} \int_0^{\Delta_*} k(E, E_*) p(E) \mathcal{F}(E, E_*) dE_* dE, \quad (20)$$

where

$$\chi \equiv \mathcal{N}/N \equiv Sv/sV. \quad (21)$$

Eqn (20) for  $f$  in combination with (9), (10), and (14) for  $p(E)$ ,  $f$ , and  $k(E, E_*)$  describes the release kinetics in the model under consideration. The right-hand part of this equation depends on  $f$  implicitly via the dependence of  $p(E)$  on  $f$  [eqn (9) and (10)]. According to eqn (20), the shape of the release kinetics is determined by the shapes of the distributions  $F(E)$  and  $\mathcal{F}(E, E_*)$ . For the timescale of release, the model yields

$$\tau \propto 1/\chi \propto V/S. \quad (22)$$

For spherically-shaped carriers, this scaling is reduced to



$$\tau \propto R. \quad (23)$$

Regarding  $\chi$  in the equations above, I can add that biologically-relevant nanocarriers can usually be classified as soft matter, and with the release of cargo their size (or volume) and structure can change. The analysis of such changes is interesting from various perspectives. In the context under consideration, this means that  $\chi$  can change with increasing time. If the heterogeneity of nanocarriers is appreciable (as assumed in my analysis), its effect on the release kinetics is expected to be much stronger than that of the change of  $\chi$ . In addition to the heterogeneity itself, one of the arguments in this favour is that the total volume of molecules transported by a nanocarrier is often appreciably smaller than that of molecules forming a nanocarrier, and the changes of the size of a nanocarrier are frequently not expected to be dramatic. For these reasons, all the structural parameters,  $R$ ,  $V$ ,  $v$ ,  $S$ , and  $s$ , used in the model are considered to be independent of time, and accordingly  $\chi$  is independent of time as well. Physically, as already articulated,  $\chi$  with its specification *via*  $V$ ,  $v$ ,  $S$ , and  $s$  is of interest in the context of carrier geometry and scaling issues [e.g., eqn (23)]. It does not, however, influence the shape of the release kinetics. Below, the presentation is focused on this shape, and accordingly  $\chi$  is considered just as a model parameter.

## B. Simplifications

In combination with (9), (10), and (14), eqn (20) is cumbersome. To facilitate its applications and understanding of the kinetics predicted, it makes sense to use three physically reasonable simplifications which may work although not always [in the latter case, one should use eqn (20)].

First, one can expect that the correlation in the distribution of  $E$  and  $E_*$  is often not of central importance, and in such cases this distribution can be factorized,

$$\mathcal{F}(E, E_*) = \Phi(E)\Phi_*(E_*), \quad (24)$$

where  $\Phi(E)$  and  $\Phi_*(E_*)$  are the partial  $E$  and  $E_*$  distributions. With this simplification and expressions (9) and (14), eqn (20) can be rewritten as

$$df/dt = -\chi k_o I_1 I_2 \exp(\mu/k_B T), \quad (25)$$

where

$$I_1 = \int_0^A \frac{\Phi(E)dE}{1 + \exp[(\mu - E)/k_B T]} \equiv 1 - \phi, \quad (26)$$

$$I_2 = \int_0^{A_*} \exp(-E_*/k_B T) \Phi_*(E_*) dE_*, \quad (27)$$

and  $\phi$  is the occupation of the sites located near the carrier-solution interface. The second integral introduced above is independent of  $f$  and  $\phi$  and accordingly does not influence the shape of the release kinetics. For this reason, it can be included into  $\chi$ . Then, substituting (26) into (25) yields

$$df/dt = -\chi k_o (1 - \phi) \exp(\mu/k_B T). \quad (28)$$

In this equation,  $\phi$  is determined by  $\Phi(E)$  and  $\mu$  [eqn (26)], and  $\mu$  is in turn determined by  $F(E)$  and  $f$  [eqn (10)].

The role of the energetic heterogeneity is appreciable if the distribution  $F(E)$  is broad. Such situations are of interest in the context of this study. In this limit, the dependence of the exponential term in eqn (25) on  $f$  is much stronger than that of  $1 - \phi$ , and accordingly  $1 - \phi$  can be safely replaced by  $1 - f$  [this replacement is fully correct provided  $F(E) = \Phi(E)$ ]. With this (second) simplification, eqn (28) is modified as

$$df/dt = -\chi k_o (1 - f) \exp(\mu/k_B T). \quad (29)$$

In this equation, as already indicated,  $\mu$  is determined by  $F(E)$  and  $f$  [eqn (10)].

Regarding eqn (28) and (29), I can repeat that they are valid provided factorization (24) of  $\mathcal{F}(E, E_*)$ . In this case, the role of the  $E_*$  distribution is reduced to the change of the timescale of the release, and it does not influence the shape of the kinetics. This case is sufficient in order to illustrate below the main special features of the kinetics under consideration. For more special goals, one can employ eqn (20) in combination with (9), (10), and (14).

If the distribution  $F(E)$  is narrow and can be neglected, the dependence of  $\mu$  on  $f$  is well known to be

$$\mu = k_B T \ln[f/(1 - f)]. \quad (30)$$

Substituting this expression into (29) yields, as expected, the conventional first-order equation,

$$df/dt = -\chi k_o f. \quad (31)$$

As already declared, I am interested in the opposite situation. In the latter case, expression (9) for  $p(E)$  can safely be replaced by the stepwise approximation,

$$p(E) = \frac{\exp[(\mu - E)/k_B T]}{1 + \exp[(\mu - E)/k_B T]} \simeq \begin{cases} 1 & \text{for } E < \mu, \\ 0 & \text{for } E > \mu, \end{cases} \quad (32)$$

With this (third) simplification, the relationship (10) between  $\mu$  and  $f$  is reduced to

$$\int_0^\mu F(E) dE = f. \quad (33)$$

Thus, eqn (29) can be solved provided the dependence  $\mu$  on  $f$  is determined by (33). This approach is used in the examples below. To compare the results of calculations with those mentioned in the introduction, the corresponding figures show the normalized amount of released drug (or vaccine),

$$\varphi(t) = \frac{M(t)}{M_\infty} = \frac{f(0) - f(t)}{f(0)}. \quad (34)$$

## III. Results of calculations

The specifics of the kinetics predicted by the model under consideration can be illustrated by employing the simplest uniform  $E$  distribution,

$$F(E) = 1/A. \quad (35)$$

In this case, eqn (33) yields



$$\mu = f\Delta, \quad (36)$$

and accordingly eqn (29) is specified as

$$df/dt = -\chi k_o(1-f)\exp(f\Delta/k_B T). \quad (37)$$

In the situations of interest, the distribution  $F(E)$  is broad ( $\Delta \gg k_B T$ ). In this limit, as already indicated, the dependence of the exponential term in eqn (37) on  $f$  is much stronger than that of  $1-f$ , and accordingly  $1-f$  can be dropped in order to explain the key features of the kinetics, *i.e.*, eqn (37) can be simplified,

$$df/dt \approx -\chi k_o \exp(f\Delta/k_B T), \quad (38)$$

and then easily integrated as

$$\exp\left(-\frac{f(t)\Delta}{k_B T}\right) - \exp\left(-\frac{f(0)\Delta}{k_B T}\right) = \frac{\chi k_o t \Delta}{k_B T}, \quad (39)$$

or

$$f(t) = -\frac{k_B T}{\Delta} \ln \left[ \exp\left(-\frac{f(0)\Delta}{k_B T}\right) + \frac{\chi k_o t \Delta}{k_B T} \right]. \quad (40)$$

The latter expression explicitly illustrates that the release kinetics are roughly linear in the very beginning provided  $\chi k_o t < (k_B T/\Delta)\exp(-f(0)\Delta/k_B T)$  and then, with increasing time, become to be logarithmic. These conclusions imply that the energy distribution is relatively broad ( $\Delta \gg k_B T$ ). In this case, both factors,  $k_B T/\Delta$  and  $\exp(-f(0)\Delta/k_B T)$ , in the condition just above are small, and accordingly the initial linear regime, occurring at  $\chi k_o t \ll 1$ , is short.

If  $1-f$  is kept in eqn (37), it can be integrated numerically. The corresponding results are presented in Fig. 1. In particular, Fig. 1(a) shows the release kinetics for  $\Delta/k_B T = 10$  and  $f(0) = 0.3, 0.5$ , and  $0.7$ . With increasing  $f(0)$ , the number of sites involved in the release increases, the range of  $E$  corresponding to these sites increases as well, and accordingly the time interval corresponding to the transition from the linear to logarithmic kinetics becomes shorter. The kinetics for  $f(0) = 0.5$  and  $\Delta/k_B T = 7, 10$ , and  $13$  are exhibited in Fig. 1(b). Here, the time interval corresponding to the transition from the linear to logarithmic kinetics becomes shorter with increasing  $\Delta/k_B T$ . This is further illustrated [Fig. 1(c)] by using a very wide energy distribution with  $\Delta/k_B T = 20$ . In this case, the initial phase of the kinetics (up to  $\varphi = 0.4$ ) is very rapid and appears to be apparently stepwise.

The linearly-increasing or decreasing  $E$  distribution can be represented as

$$F(E) = \frac{A}{\Delta} + \frac{2(1-A)E}{\Delta^2}, \quad (41)$$

where  $A$  is the corresponding parameter. Substituting this expression into the left-hand part of eqn (33) and calculating the integral there yields

$$\frac{A\mu}{\Delta} + \frac{(1-A)\mu^2}{\Delta^2} = f, \quad (42)$$

or

$$\mu = \{A/2 - [A^2/4 + (1-A)f]^{1/2}\}\Delta/(A-1). \quad (43)$$

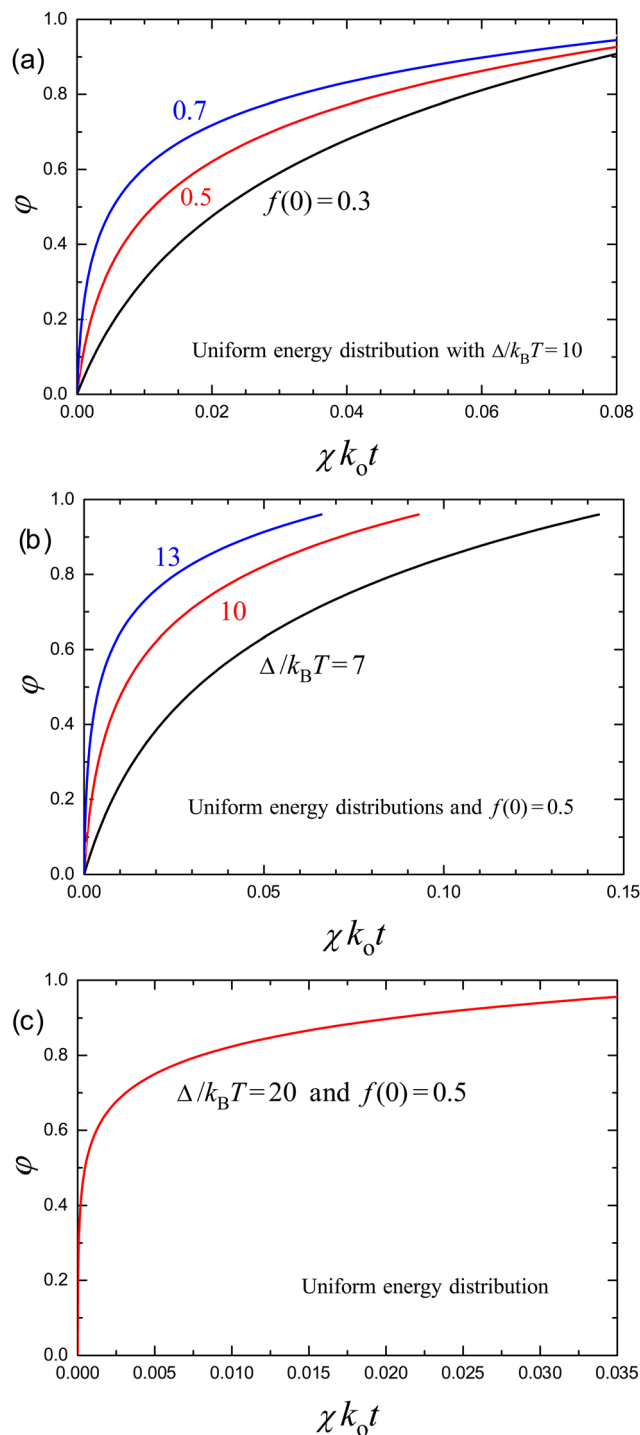


Fig. 1 Kinetics of release of molecules from a carrier according to eqn (37) in the case of uniform distribution of sites over energy [eqn (35)] for (a)  $\Delta/k_B T = 10$  and  $f(0) = 0.3, 0.5$ , and  $0.7$ ; (b)  $f(0) = 0.5$  and  $\Delta/k_B T = 7, 10$ , and  $13$ ; and (c)  $f(0) = 0.5$  and  $\Delta/k_B T = 20$ .

The release kinetics calculated by using eqn (29) in combination with (43) are presented in Fig. 2 for  $f(0) = 0.5$ ,  $\Delta/k_B T = 10$ , and  $A = 0.7, 1$ , and  $1.3$ . Here, with increasing  $A$ , the range of  $E$  corresponding to the sites involved in the release decreases,





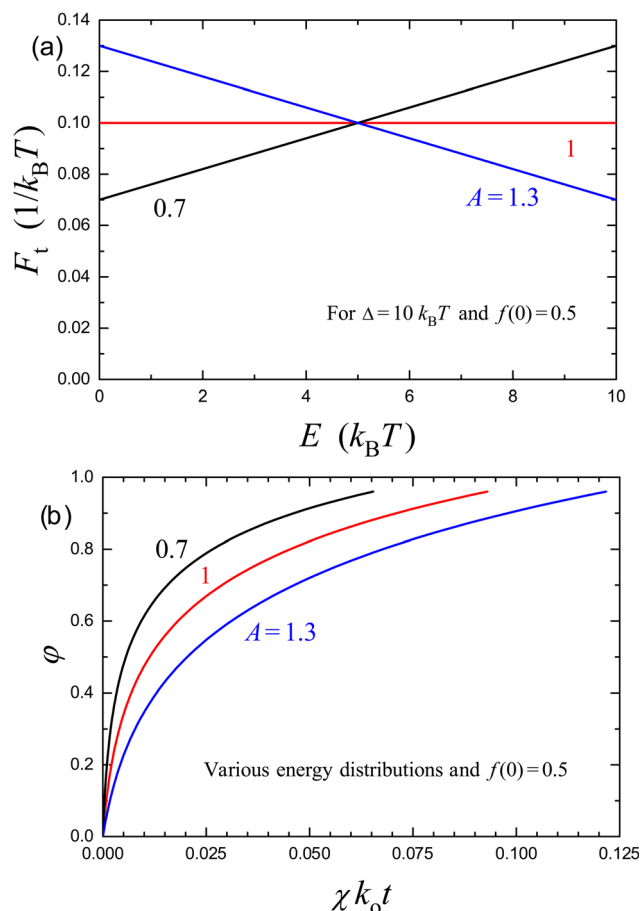


Fig. 2 (a) Monotonously increasing, uniform, and monotonously decreasing distributions of site energies [eqn (41) with  $\Delta/k_B T = 10$  and  $A = 0.7, 1$ , and  $1.3$ , respectively], and (b) the corresponding kinetics of release of molecules from a carrier for  $f(0) = 0.5$  according to eqn (29) in combination with (43).

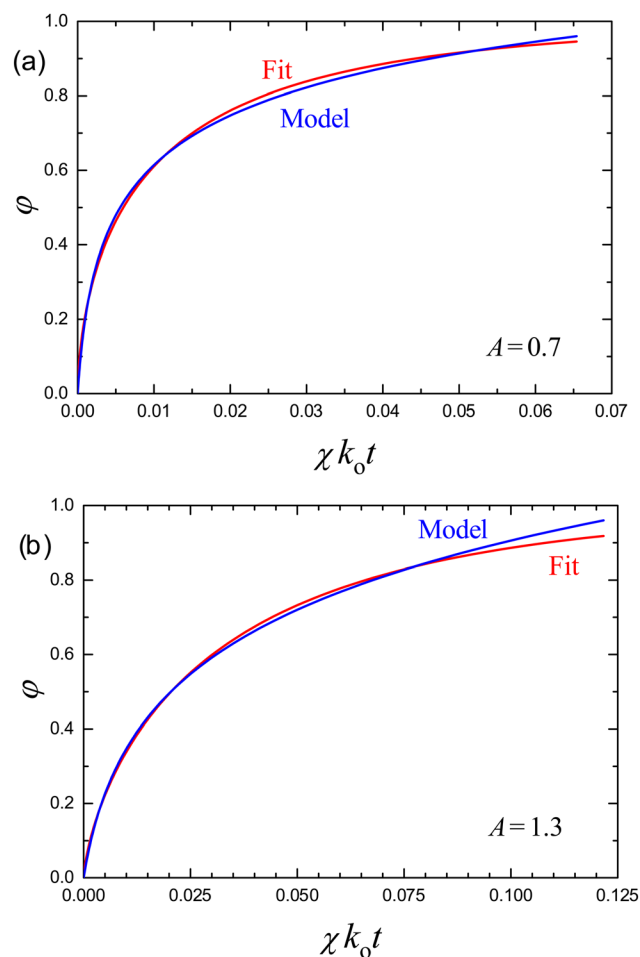


Fig. 3 Fit of the two kinetics shown in Fig. 2(b) with  $A = 0.7$  (a) and  $1.3$  (b) by using the Weibull expression [eqn (4)] with  $\alpha = 0.6$  and  $0.72$ , respectively.

and the time interval corresponding to the transition from the linear to logarithmic kinetics becomes longer.

To link the results presented with those available in the literature, the two kinetics shown in Fig. 2 (for  $A = 0.7$  and  $1.3$ ) have been fitted (Fig. 3) by employing the Weibull expression [eqn (4)]. The fit is nearly perfect in the whole range of  $\phi$  provided the exponent  $\alpha$  is set to  $0.60$  and  $0.72$ , respectively. In fact, the difference between the curves is smaller than the typical error bar in the corresponding experimentally measured kinetics (for the latter, see *e.g.* Section IV below). Thus, the model proposed and the Weibull expression are formally equivalent in the context of fitting the experimentally observed kinetics. The Weibull expression is, however, axiomatic, whereas the model proposed can help to clarify the physics of the systems under consideration.

The conclusions above are applicable also to the fit by the Korsmeyer–Peppas expression [eqn (5)] which can be obtained by expansion of the Weibull expression and accordingly can safely be used provided  $\phi$  is not too close to unity. In the whole range of  $\phi$ , the accuracy of the Korsmeyer–Peppas expression is somewhat worse compared to that of the Weibull expression.

Regarding this aspect, I can add that in experiments the range of  $\phi$  is typically somewhat smaller than that shown in Fig. 3. One of the reasons might be that due to the logarithmic slowdown the kinetics cannot always be tracked up to  $\phi = 1$ . In such situations, the accuracy of the Korsmeyer–Peppas expression is somewhat better. If the time interval in the model kinetics shown in Fig. 3 is reduced, their fit by employing the Korsmeyer–Peppas expression provides  $\alpha$  values slightly smaller or larger than those corresponding to the Weibull expression. Concerning the obtained exponents,  $\alpha = 0.60$  and  $0.72$ , I can add that the two kinetics shown in Fig. 2 and used for fitting in Fig. 3 were calculated with  $\Delta/k_B T = 10$ . With increasing  $\Delta/k_B T$ ,  $\alpha$  will be smaller.

The fact that the kinetics predicted by the model under consideration can be well fitted by using the Weibull or Korsmeyer–Peppas expression (Fig. 3) is a consequence of the choice of the energy distributions which are relatively broad and monotonous. The corresponding kinetics (Fig. 2 and 3) have been calculated by using eqn (29) in combination with (43). The model in its general form [eqn (20) in combination with (9), (10), and (14)] or more simple eqn (29) in combination



with (10) or (33) are applicable to other energy distributions as well.

For example, the simplest alternative distribution is that for sites of two types with energies  $E_1 = 0$  and  $E_2 = \Delta$ , so that eqn (10) is reduced to

$$f = \frac{\theta_1 \exp(\mu/k_B T)}{1 + \exp(\mu/k_B T)} + \frac{\theta_2 \exp[(\mu - \Delta)/k_B T]}{1 + \exp[(\mu - \Delta)/k_B T]}, \quad (44)$$

where  $\theta_1$  and  $\theta_2$  are the fractions of these sites ( $\theta_1 + \theta_2 = 1$ ). If a system is heterogeneous and the difference between these energies is about  $5k_B T$  or larger, the model will predict very rapid release corresponding to one energy followed by much slower release corresponding to another energy (Fig. 4). The important point is that these two subkinetics are nearly separated because the corresponding time scales are very different, and accordingly the fit by the Weibull or Korsmeyer–Peppas expression will not work. If the energy distributions are relatively broad and monotonous as considered in my analysis above (e.g., Fig. 2 and 3), the separation of the kinetics at high and low occupation of sites (i.e., in the regimes with domination of sites with low and high binding energies, respectively) is smeared by the kinetics at an intermediate occupation of sites (i.e., in the regime with domination of sites with moderate binding energies), and mathematically this results in logarithmic features.

Of note, the logarithmic kinetics related to a broad distribution of kinetic parameters were previously experimentally observed and theoretically analyzed in various branches of natural sciences. For example, I refer to the studies focused on the kinetics of adsorption on and desorption from heterogeneous surfaces with distribution of binding and activation energies,<sup>33</sup> electron transport in nanocrystalline semiconductor films,<sup>34</sup> and electron tunneling at low temperatures in arrays of immobile donors and acceptors or arrays of donors–acceptor pairs with appreciable

distribution of distances between donors and acceptors.<sup>35</sup> To some extent, the description of adsorption on and desorption from heterogeneous surfaces is similar to what I present. The difference is that these processes occur exclusively at surface sites, whereas the release under consideration occurs from the sites located near the interface and the occupation of these sites is, in fact, dictated by the occupation of sites located inside a carrier. For this reason, the details of the math are different. For instance, the key general equation derived in my work is (20). I have simplified it down to (37) for the calculations shown in Fig. 1. For qualitative illustration, I have further simplified (37) down to (38). The latter equation is e.g. similar (except the sign and designations) to eqn (1) presented in ref. 33 for describing the kinetics of adsorption. The corresponding kinetics (eqn (40) in my case and eqn (2) in ref. 33) exhibit similar logarithmic features.

## IV. Related experimental results

Regarding the comparison of the model predictions with the results of available experiments, I can repeat (cf. the introduction) that the Weibull and Korsmeyer–Peppas expressions were/are very widely employed for fitting the observed release kinetics. Many suitable examples can be found with the corresponding references e.g. in the review published in 2019 by Mircioiu *et al.*<sup>7</sup> (see Tables 1, 2 and 4 for micro- and nano-sized carriers). The range of the exponents collected there is rather large,  $0.45 \leq \alpha \leq 0.85$ .

Aiming at more recent experiments, one can employ “Korsmeyer–Peppas” as search words in e.g. Sci. Cit. Ind. It yields a few hundred examples of the use of the corresponding expression for fitting the observed kinetics of release from various carriers. Several relevant recent studies (ref. 36–47) reporting typical values of  $\alpha$  are as follows.

Alinavaz *et al.*<sup>36</sup> explored magnetic carboxymethylcellulose/chitosan bio-nanocomposites of  $\sim 50$  nm size for smart co-delivery of sunitinib malate anticancer compound and saffron extract.  $\alpha$  is reported to be in the range from 0.30 to 0.60.

Altom *et al.*<sup>37</sup> used cellulose fibers/zeolite-A biocomposites of  $\sim 100$ – $200$  nm size as a carrier of oxaliplatin drug.  $\alpha$  is reported to be in the range from 0.53 to 0.70.

Ge *et al.*<sup>38</sup> studied magadiite-sodium alginate drug carrier composites of different shapes and sizes.  $\alpha$  is reported to be in the range from 0.40 to 0.66.

Gilani *et al.*<sup>39</sup> explored osimertinib nano lipid carriers of  $\sim 150$  nm size.  $\alpha$  is reported to be 0.43.

Haseli *et al.*<sup>40</sup> used release of curcumin from chitosan-based carriers of  $\sim 100$  nm size.  $\alpha$  is reported to be 0.78 and 1.01.

Luo *et al.*<sup>41</sup> explored sorafenib-loaded LNPs of  $\sim 100$  nm size for *in vitro* and *in vivo* studies in the context of topical ocular therapy of corneal neovascularization.  $\alpha$  is reported to be 0.44 and 0.97.

Ozkahraman *et al.*<sup>42</sup> employed *N*-vinylcaprolactam and methacrylic acid based hydrogels (with the heterogeneity on the scale of  $\sim 1$   $\mu$ m) in the context of drug release.  $\alpha$  is reported to be in the range from 0.40 to 0.56.

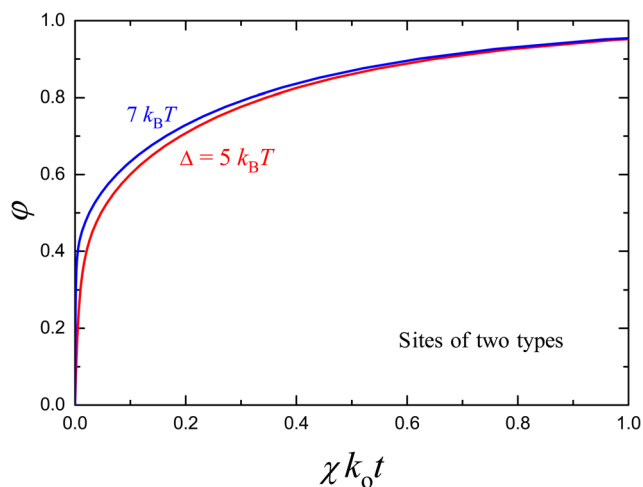


Fig. 4 Kinetics of the release of molecules from a carrier containing absorption sites of two types with  $E_1 = 0$  and  $E_2 = \Delta$ , according to eqn (29) and (44) with  $f(0) = 0.8$ ,  $\theta_1 = \theta_2 = 0.5$ , and  $\Delta = 5$  and  $7k_B T$ . In both cases, the initial phase of the kinetics (up to  $\phi = 0.4$ ) is very rapid. For  $\Delta = 7k_B T$ , this phase is apparently stepwise [as in Fig. 1(c)]. These kinetics are poorly fitted by the Weibull and Korsmeyer–Peppas expressions.



Qiao *et al.*<sup>43</sup> used silk fabric decorated with hydrogel (with the heterogeneity on the scale up to  $\sim 10\ \mu\text{m}$ ) for sustained release of paracetamol.  $\alpha$  is reported to be 0.66 and 0.68.

Truong *et al.*<sup>44</sup> employed  $\sim 150\ \text{nm}$ -sized LNPs as carriers for *Capsicum* oleoresin.  $\alpha$  is reported to be 0.86.

Truong *et al.*<sup>45</sup> also used  $\sim 250\ \text{nm}$ -sized chitosan-coated LNPs for transdermal delivery of tetrahydrocurcumin.  $\alpha$  is reported to be 0.36 and 0.66.

Velez-Pena *et al.*<sup>46</sup> employed mesoporous mixed oxides of  $\sim 700\text{--}1100\ \text{nm}$  size as drug delivery carriers for methotrexate.  $\alpha$  is reported to be in the range from 0.49 to 0.62.

Yildirim and Dogac<sup>47</sup> studied the release of 5-fluorouracil from magnetic  $\text{MnFe}_2\text{O}_4$ /alginate beads in the context of cancer drug delivery.  $\alpha$  is reported to be in the range from 0.43 to 0.62.

In agreement with the previous studies reviewed by Mircioiu *et al.*,<sup>7</sup> recent studies (ref. 36–47) focused on various cargos and carriers show that  $\alpha$  is often in the range from 0.45 to 0.85. As I have illustrated in Section III, the Weibull and Korsmeyer–Peppas expressions with this range of  $\alpha$  can easily be reproduced by using the model under consideration with appreciable heterogeneity. Thus, this model can be used to fit numerous experimentally measured kinetics and the fit will obviously good. This means that the model is formally applicable to the corresponding real systems and can be potentially applicable to many other systems.

## V. Conclusions

The kinetics of drug or vaccine release from carriers are of high interest from various perspectives. With decreasing the carrier size down to  $\sim 100\ \text{nm}$  and using the biologically-inspired soft-matter carriers, the timescale of diffusion of drug or vaccine molecules is shortened, and the release kinetics are likely to be kinetically limited. I have presented the generic kinetic model describing this regime of release and allowing one to take the energetic heterogeneity into account (Section II). In the absence of heterogeneity, the model is reduced to the first-order equation resulting in exponential kinetics. In the calculations illustrating the effect of heterogeneity on the corresponding kinetics (Section III), the deviation of the molecule binding from the minimal value was considered to be  $\sim 7\text{--}13k_{\text{B}}T$  ( $4\text{--}8\ \text{kcal mol}^{-1}$ ). Roughly, this is about one third or fourth of the likely activation barrier for release. With this physically reasonable (for non-covalent interaction) scale of heterogeneity, the predicted kinetics (i) are linear in the very beginning and then, with increasing time, become logarithmic and (ii) can be nearly perfectly fitted by using the empirical Weibull or Korsmeyer–Peppas expressions with the exponent  $\alpha$  in the range from 0.6 (or somewhat lower) to 0.75. Taken together, the result obtained (Section III) indicates that in terms of the conventional empirical expressions the kinetics predicted by model I use can formally be characterized by  $\alpha$  in the range from 0.6 (or somewhat lower) to 1. The values of  $\alpha$  obtained here for energetically heterogeneous carriers [from 0.6 (or somewhat lower) to 0.75] are usually associated with non-Fickian diffusion. The model presented shows that the energetic heterogeneity can be operative in these cases as well.

The range of the values of  $\alpha$  predicted by the model under consideration is in agreement with that observed in experiments (Section IV). From this perspective, the model is practically relevant. Whether or not the model is really applicable and whether or not it is preferable compared to the other available models should be clarified *e.g.* by exploring the specifics of the structure of micro- or nanocarriers and simultaneously measuring the rate of diffusion of drug or vaccine molecules inside and comparing the diffusion time scale with that of release. Such measurements are challenging and now lacking (see, *e.g.*, the already mentioned recent studies<sup>36–47</sup>).

Regarding the applicability of the model to the biologically-inspired soft-matter nanocarriers, one should bear in mind that it operates with a fixed number of sites and distributions of energies of molecules bound at sites. Soft-matter nanocarriers (*e.g.*, LNPs) are expected to be dynamic and the number of sites and distributions of sites over energy can vary in the course of release. The model is applicable provided the corresponding variations are modest.

The model does not take the interaction between molecules into account. At the mean-field level, this interaction is well known to be described by introducing the linear term,  $Cf$  ( $C$  is a constant proportional to the interaction energy), into the chemical potential. If needed, this modification can easily be incorporated into the equations presented in Sections II and III. Often, this is a matter of redefinition of some of the parameters. At a higher level, the inclusion of the interaction between molecules should be made in parallel with that of the correlation between the location of sites with different energies, and it results in cumbersome equations which can be analyzed only numerically.

Finally, I add two general remarks in order to extend slightly the scope of the discussion above:

(i) The kinetic models briefly outlined in the introduction were originally proposed primarily in the context of drug release from macroscopic pellets. The model treated in my work has been motivated by referring to biologically-inspired nanocarriers. It is expected to be applicable to experiments performed both *in vitro* and *in vivo*. The situations *in vivo* can be much richer than those described by the models mentioned. For example, the intracellular release from LNPs may occur during their interaction with lipid membranes (*e.g.*, at anionic membranes of endosomes). The corresponding concepts are now available<sup>48,49</sup> whereas the suitable kinetic models are lacking in fact (see *e.g.* the discussion in ref. 29).

(ii) With minor modifications the treatment presented in this study can be used to describe systems which were not mentioned above. In nanoscience, for example, the release of hydrogen from alloyed metal nanoparticles attracts nowadays attention from various perspectives.<sup>50</sup> In the context of hydrogen absorption, such particles are energetically heterogeneous. The  $\text{H}_2$  release occurs *via* associative desorption of hydrogen from the surface, whereas the hydrogen surface coverage is controlled by hydrogen absorbed inside. The corresponding absorption isotherms have already been analyzed theoretically,<sup>51</sup> whereas the treatment of the release kinetics taking the heterogeneity into





account is still lacking. With some modifications, it can be done by using the formalism presented.

## Conflicts of interest

There are no conflicts to declare.

## Acknowledgements

The author thanks Prof. F. Höök for useful discussions. The work was supported by the Ministry of Science and Higher Education of the Russian Federation within the governmental order for Bor-  
eskov Institute of Catalysis (project AAAA-A21-121011390008-4).

## References

- 1 S. Agrawal, J. Fernandes, F. Shaikh and V. Patel, Quality aspects in the development of pelletized dosage forms, *Heliyon*, 2022, **8**, e08956.
- 2 M. S. Handattu, S. Thirumaleshwar, G. M. Prakash, H. K. Somareddy and G. H. Veerabhadrapa, A comprehensive review on pellets as a dosage form in pharmaceuticals, *Curr. Drug Targets*, 2021, **22**, 1183–1195.
- 3 T. Chen, J. Li, T. Chen, C. C. Sun and Y. Zheng, Tablets of multi-unit pellet system for controlled drug delivery, *J. Controlled Release*, 2017, **262**, 222–231.
- 4 M. J. Mitchell, M. M. Billingsley, R. M. Haley, M. E. Wechsler, N. A. Peppas and R. Langer, Engineering precision nanoparticles for drug delivery, *Nat. Rev. Drug Discovery*, 2021, **20**, 101–124.
- 5 X. Hou, T. Zaks, R. Langer and Y. Dong, Lipid Nanoparticles for mRNA delivery, *Nat. Rev. Mater.*, 2021, **6**, 1078–1094.
- 6 J. A. Jackman, *et al.*, Antiviral therapies and vaccines, *Adv. Funct. Mater.*, 2020, **31**, 2008352.
- 7 C. Mircioiu, *et al.*, Mathematical modeling of release kinetics from supramolecular drug delivery systems, *Pharm.*, 2019, **11**, 140.
- 8 N. A. Peppas and B. Narasimhan, Mathematical models in drug delivery: How modeling has shaped the way we design new drug delivery systems, *J. Controlled Release*, 2014, **190**, 75–81.
- 9 J. Siepmann and F. Siepmann, Modeling of diffusion controlled drug delivery, *J. Controlled Release*, 2012, **161**, 351–362.
- 10 A. Hadjithodorou and G. Kalosakas, Quantifying diffusion-controlled drug release from spherical devices using Monte Carlo simulations, *Mater. Sci. Eng., C*, 2013, **33**, 763–768.
- 11 W. Weibull, A statistical distribution function of wide applicability, *ASME J. Appl. Mech.*, 1951, 293–297.
- 12 V. Papadopoulou, K. Kosmidis, M. Vlachou and P. Macheras, On the use of the Weibull function for the discernment of drug release mechanisms, *Int. J. Pharm.*, 2006, **309**, 44–50.
- 13 R. W. Korsmeyer, R. Gurny, E. Doelker, P. Buri and N. A. Peppas, Mechanisms of solute release from porous hydrophilic polymers, *Int. J. Pharm.*, 1983, **15**, 25–35.
- 14 J. Siepmann and F. Siepmann, Mathematical modeling of drug dissolution, *Int. J. Pharm.*, 2013, **453**, 12–24.
- 15 K. Kosmidis, P. Argyrakis and P. Macheras, A reappraisal of drug release laws using Monte Carlo simulations: the relevance of the Weibull function, *Pharm. Res.*, 2003, **20**, 988–995.
- 16 T. I. Spiridonova, S. I. Tverdokhlebov and Y. G. Anissimov, Investigation of the size distribution for diffusion-controlled drug release from drug delivery systems of various geometries, *J. Pharm. Sci.*, 2019, **108**, 2690–2697.
- 17 E. J. Carr and G. Pontrelli, Modelling mass diffusion for a multi-layer sphere immersed in a semi-infinite medium: application to drug delivery, *Math. Biosci.*, 2018, **303**, 1–9.
- 18 E. J. Carr and G. Pontrelli, Drug delivery from microcapsules: How can we estimate the release time?, *Math. Biosci.*, 2019, **315**, 108216.
- 19 G. Pontrelli, E. J. Carr, A. Tiribocchi and S. Succi, Modeling drug delivery from multiple emulsions, *Phys. Rev. E*, 2020, **102**, 023114.
- 20 A. Jain, S. McGinty, G. Pontrelli and L. Zhou, Theoretical model for diffusion-reaction based drug delivery from a multilayer spherical capsule, *Int. J. Heat Mass Transfer*, 2022, **183**, 122072.
- 21 S. Mubarak and M. A. Khanday, Mathematical modelling of drug-diffusion from multi-layered capsules/tablets and other drug delivery devices, *Comput. Meth. Biomech. Biomed. Eng.*, 2022, **25**, 896–907.
- 22 P. Macheras and A. Dokoumetzidis, On the heterogeneity of drug dissolution and release, *Pharm. Res.*, 2000, **17**, 108–112.
- 23 K. Kosmidis and P. Macheras, Monte Carlo simulations for the study of drug release from matrices with high and low diffusivity areas, *Int. J. Pharm.*, 2007, **343**, 166–172.
- 24 P. D. Mavroudis, K. Kosmidis and P. Macheras, On the unphysical hypotheses in pharmacokinetics and oral drug absorption: time to utilize instantaneous rate coefficients instead of rate constants, *Eur. J. Pharm. Sci.*, 2019, **130**, 137–146.
- 25 J. A. Maroto-Centeno and M. Quesada-Perez, Coarse-grained simulations of diffusion controlled release of drugs from neutral nanogels: effect of excluded volume interactions, *J. Chem. Phys.*, 2020, **152**, 024107.
- 26 V. P. Zhdanov, Intracellular RNA delivery by lipid nanoparticles: diffusion, degradation, and release, *BioSystem*, 2019, **185**, 104032.
- 27 A. Jain, S. McGinty and G. Pontrelli, Drug diffusion and release from a bioerodible spherical capsule, *Int. J. Pharm.*, 2022, **616**, 121442.
- 28 M. S. Gomes-Filho, F. A. Oliveira and M. A. A. Barbosa, Modeling the diffusion-erosion crossover dynamics in drug release, *Phys. Rev. E*, 2022, **105**, 044110.
- 29 V. P. Zhdanov, Lipid nanoparticles with ionizable lipids: statistical aspects, *Phys. Rev. E*, 2022, **105**, 044405.
- 30 M. A. Oberli, *et al.*, Immunotherapy, *Nano Lett.*, 2017, **17**, 1326–1335.
- 31 S. S. W. Leung and C. Leal, The stabilization of primitive bicontinuous cubic phases with tunable swelling over a wide composition range, *Soft Matter*, 2019, **15**, 1269–1277.
- 32 N. Y. Arteta, *et al.*, Successful reprogramming of cellular protein production through mRNA delivered by functionalized lipid nanoparticles, *Proc. Natl. Acad. Sci. U. S. A.*, 2018, **115**, E3351–E3360.



- 33 I. S. McIntock, The Elovich equation in chemisorption kinetics, *Nature*, 1967, **216**, 1204–1205.
- 34 J. Nelson, Continuous-time random-walk model of electron transport in nanocrystalline TiO<sub>2</sub> electrodes, *Phys. Rev. B: Condens. Matter Mater. Phys.*, 1999, **59**, 15374–15380.
- 35 R. F. Khairutdinov, K. I. Zamaraev and V. P. Zhdanov, *Electron Tunneling in Chemistry*, Elsevier, Amsterdam, 1989.
- 36 S. Alinavaz, *et al.*, Novel magnetic carboxymethylcellulose/chitosan bio-nanocomposites for smart co-delivery of sunitinib malate anticancer compound and saffron extract, *Polym. Intern.*, 2022, **71**, 1243–1251.
- 37 N. Altoom, *et al.*, Insight into the loading, release, and anticancer properties of cellulose/zeolite-A as an enhanced delivery structure for oxaliplatin chemotherapy; characterization and mechanism, *J. Sol-Gel Sci. Technol.*, 2022, **103**, 752–765.
- 38 M. Ge, *et al.*, Preparation of magadiite-Sodium alginate drug carrier composite by pickering-emulsion-templated-encapsulation method and its properties of sustained release mechanism by Baker-Lonsdale and Korsmeyer-Peppas model, *J. Polym. Environ.*, 2022, **30**, 3890–3900.
- 39 S. J. Gilani, *et al.*, Formulation of osimertinib nano lipid carriers: optimization, characterization and cytotoxicity assessment, *J. Cluster Sci.*, 2023, **34**, 1051–1063.
- 40 S. Haseli, *et al.*, A novel pH-responsive nanoniosomal emulsion for sustained release of curcumin from a chitosan-based nanocarrier: Emphasis on the concurrent improvement of loading, sustained release, and apoptosis induction, *Biotechnol. Prog.*, 2022, **38**, e3280.
- 41 Q. Luo, *et al.*, Sorafenib-loaded nanostructured lipid carriers for topical ocular therapy of corneal neovascularization: development, *in-vitro* and *in vivo* study, *Drug Delivery*, 2022, **29**, 837–855.
- 42 B. Özkahraman, I. Acar and G. Guclu, Synthesis of N-vinylcaprolactam and methacrylic acid based hydrogels and investigation of drug release characteristics, *Polym. Bull.*, 2023, **80**, 5149–5181.
- 43 N. Qiao, *et al.*, Silk fabric decorated with thermo-sensitive hydrogel for sustained release of paracetamol, *Macromol. Biosci.*, 2022, 2200029.
- 44 C. T. Truong, *et al.*, Development of topical gel containing Capsicum oleoresin encapsulated Tamanu nanocarrier and its analgesic and anti-inflammatory activities, *Mater. Today Commun.*, 2022, **31**, 103404.
- 45 T. H. Truong, *et al.*, Chitosan-coated nanostructured lipid carriers for transdermal delivery of tetrahydrocurcumin for breast cancer therapy, *Carbohydr. Polym.*, 2022, **288**, 119401.
- 46 E. Velez-Pena, *et al.*, Mesoporous mixed oxides prepared by hard template methodology as novel drug delivery carriers for methotrexate, *J. Drug Deliv. Sci. Technol.*, 2022, **73**, 103483.
- 47 A. Yildirim and Y. I. Dogac, MnFe<sub>2</sub>O<sub>4</sub>/alginate magnetic beads as platform for cancer drug delivery: an in vitro study of 5-fluorouracil release, *J. Macromol. Sci. A Pure Appl. Chem.*, 2022, **59**, 558–566.
- 48 S. A. Smith, L. I. Selby, A. P. R. Johnston and G. K. Such, The endosomal escape of nanoparticles: toward more efficient cellular delivery, *Bioconjugate Chem.*, 2019, **30**, 263–272.
- 49 I. M. S. Degors, C. Wang, Z. U. Rehman and I. S. Zuhorn, Carriers break barriers in drug delivery: endocytosis and endosomal escape of gene delivery vectors, *Acc. Chem. Res.*, 2019, **52**, 1750–1760.
- 50 F. A. A. Nugroho, *et al.*, Metalpolymer hybrid nanomaterials for plasmonic ultrafast hydrogen detection, *Nat. Mater.*, 2019, **18**, 489–495.
- 51 M. Mamatkulov and V. P. Zhdanov, Partial or complete suppression of hysteresis in hydride formation in binary alloys of Pd with other metals, *J. Alloys Compd.*, 2021, **885**, 160956.

